Primerjava lokalnih geoidnih modelov v zahodni Makedoniji, določenih z metodama KTH in CSH

Comparison of Local Geoid Models in Western Macedonia Determined by KTH and CSH Methods

Filip Petrovski, Zlatko Bogdanovski

UDK: 528.21:004.925.8
Klasifikacija prispevka po COBISS.SI: 1.01
Prispelo: 12. 8. 2025
Sprejeto: 15. 1. 2026

DOI: https://doi.org/10.15292/geodetski-vestnik.2026.02.248-267
SCIENTIFIC ARTICLE
Received: 12. 8. 2025
Accepted: 15. 1. 2026

IZVLEČEK

Eden temeljnih ciljev geodezije je določitev modela geoida za posamezno regijo, bodisi lokalno bodisi globalno. Raziskava obravnava ključne teoretične, metodološke in numerične izzive pri modeliranju geoida ter opisuje model geoida za območje v zahodni Makedoniji z uporabo metod KTH in CSH. Analiza združuje globalne geopotencialne modele (GGM), digitalne modele višin (DMV), anomalije težnosti in podatke GNSS. GGM in DMV so prosto dostopni, medtem ko je nabore podatkov o gravitaciji in GNSS zagotovila Agencija za kataster Severne Makedonije (AREC). V raziskavi smo uporabili sedem samo satelitskih modelov GGM (GOCE, GRACE in GOCE+GRACE) ter kombinirani model EGM2008. Za izračune so bili uporabljeni javno dostopni modeli DMV (SRTM, ASTER, MERIT in TANDEM-X). Za izračun anomalije težnosti smo uporabili meritve iz kampanje AREC (2010–2014) ter zgodovinske podatke SFRJ iz šestdesetih in sedemdesetih let prejšnjega stoletja. Nabor podatkov dodatno vsebuje 61 GNSS/nivelman točk in 104 dodatne gravimetrične točke, kar skupaj znaša 165. Od GNSS točk jih je bilo 46 uporabljenih za validacijo modelov.

Po izračunu so bili modeli gravimetričnega geoida vključeni v višinski sistem regije z uporabo štiriparametrične transformacijske ploskve. Primerjava izračunanih modelov pred vklopom in po njem je z metodama KTH oziroma CSH dala povprečni pogrešek RMSE 5,53 centimetra oziroma 5,51 centimetra.

KLJUČNE BESEDE

geoid, težnost, KTH, CSH, GNSS, nivelman, GGM, DMV

ABSTRACT

One of the fundamental objectives in geodesy is determining a geoid model for a specific region, whether local or global. The research addresses key theoretical, methodological, and numerical challenges in geoid modelling and presents a geoid for a specific region in Western Macedonia, using the KTH and CSH methods.

The analysis integrates global geopotential models (GGMs), digital elevation models (DEMs), gravity anomalies, and GNSS data. The GGMs and DEMs are freely accessible, whereas the gravity and GNSS datasets were obtained from the Agency for Cadastre of North Macedonia (AREC). Seven GGMs chosen are satellite-only (GOCE, GRACE, and GOCE+GRACE) and the combined model EGM2008 to analyze different model behaviors. The publicly available DEMs (SRTM, ASTER, MERIT, and TANDEM-X) were used for the calculations.

Gravity data include measurements from an AREC campaign (2010-2014) and historical SFRY data from the 1960s-1970s. The dataset contains 61 GNSS/levelling points and 104 additional gravity points, totalling 165. Of the GNSS ponts, 46 were used for validation of the models.

Following computation, the gravimetric geoids were fitted using a four-parameter corrector surface. Comparison of gravimetric and geometric undulations yielded root mean square errors (RMSE) of 5.53 cm and 5.51 cm, with KTH and CSH methods, respectively.

KEY WORDS

Geoid, Gravity, KTH, CSH, GNSS, Levelling, GGM, DEM

1 Introduction

GNSS surveys provide horizontal positions and ellipsoidal heights, which quantify absolute elevations relative to the WGS84 reference ellipsoid. While the ellipsoidal heights (h) are absolute in a geometric sense, they do not directly represent physical heights above sea level. At locations where GNSS measurements are taken, the availability of independently determined orthometric heights (H) allows us to establish a direct relationship between geometric and physical height systems. The present study focuses on integrating geometric and physical height systems using gravity data. Similar studies implementing both methods have been conducted in the past: Croatian geoid model using KTH method with accuracy of 3.5 cm (Varga, 2018), KTH geoid model for Bosnia & Herzegovina yielding an error of 5.6 cm (Krdžalić & Abbak, 2023), CSH geoid model for Auvergne region in France with error of 2.7 cm (R. A. Abbak *et al.*, 2024), comparison of KTH method (RMSE=6.7 cm) and CSH method (RMSE=9.8 cm) for Konya closed basin (R. A. Abbak *et al.*, 2012). The goal is to compute the geoid undulation (N), defined as N = h – H. Terrestrial gravity data capture ultra-short-wavelength variations. However, gravimetric geoid models require both short- and long-wavelength components to achieve accuracy. DEMs are employed to represent short-wavelength features, while GGMs account for long-wavelength variations. DEMs are generated by various institutions through multiple satellite missions, whereas GGMs are collected and archived by the International Centre for Global Earth Models (ICGEM) (Ince *et al.*, 2019).

The analysis commences with the regional characterization of the study area, followed by a comprehensive review of the datasets employed. The primary data sources include GGMs, whose validation was conducted using GNSS/levelling points prior to their application. Comparable studies have been performed worldwide. For instance, GGM validation in Nigeria, conducted over 90 GNSS/levelling points, yielded a standard deviation of 0.31 cm using a four-parameter fit (Bako *et al.*, 2025). Similarly, the validation of GOCE-only models in Poland produced STDs ranging from 2.8 cm to 3.4 cm when compared with GNSS/levelling data and 0.84 mGal when compared with terrestrial free-air gravity anomalies (Godah *et al.*, 2015). An evaluation of GGMs over the internal Aegean region of Turkey, based on 87 control points, resulted in RMS error of 0.34 cm after applying a four-parameter fit (Yilmaz *et al.*, 2016). Another essential dataset utilized in this study comprises DEMs, which were assessed against levelling data to evaluate their accuracy. Similar investigations include the comparison of ASTER and SRTM DEMs in Turkey (Bildirici & Abbak, 2017), the evaluation of DEM accuracy in the Auvergne region—where SRTM achieved an RMS of 2.02 m and ASTER had an RMS of 4.70 m when compared with GNSS/levelling points (R. A. Abbak, 2014), and the assessment of the TanDEM-X model in Malaysia using 45 GNSS/levelling points (Halim *et al.*, 2019). The subsequent chapters provide a detailed discussion of the geoid determination methodologies, highlighting both their theoretical foundations and practical implementation. The final chapter presents the derived geoid models and their corresponding accuracy assessment based on RMS error analysis. Additionally, a visual representation of the resulting geoid model is included, illustrating the spatial variation of the geoid and supporting the evaluation of its overall precision.

2 Study area for local geoid

The study area selected for the development of a local geoid model is situated in the northwestern region of North Macedonia, bounded by $\varphi_{min} = 41°18'18"$ to $\varphi_{max} = 41°38'42"$ north latitude and $\lambda_{min} = 20°39'18"$ to $\lambda_{max} = 20°59'42"$ east longitude. This region was chosen due to its dynamic topography, with elevations

ranging from a minimum of 594 m to a maximum of 2102 m above sea level, and an average altitude of approximately 1264 m.

Historically, gravity surveys in the territory of the former Yugoslavia, including present-day North Macedonia, were conducted during the 1960s and 1970s by the Military Geographical Institute from Belgrade. This initial national campaign resulted in a network of 3,587 gravity points across North Macedonia. The gravity survey was conducted by establishing 15 stations forming a first-order gravity network. The network was subsequently densified through the establishment of a basic network consisting of 55 polygons with a total approximate length of 370 km. The primary vector baselines of this network were the short baseline Avala and the long baseline Belgrade–Skopje. Measurements were carried out using a North American AGL gravimeter, employing the STEP method. The standard deviation of the basic network is approximately 0.02 mGal, indicating high measurement precision. All gravity observations were originally referenced to the Potsdam gravity system. In terms of positioning, the data are referenced to the former Yugoslav national coordinate system, with the horizontal datum defined by the Hermannskogel fundamental point in Austria and based on the Bessel ellipsoid.

More recently, a comprehensive gravity campaign was undertaken in 2010 to establish a modern gravimetric infrastructure. This effort included the establishment of an absolute gravity network of the zero-order, with measurements at three fundamental stations (Skopje, Ohrid, and Valandovo), with accuracy of 3 μGal. The network was subsequently densified with a first-order network comprising 25 points (accuracy of 13 μGal) and a second-order network of 2,310 points (accuracy of around 60 μGal) (Gospodinov *et al.*, 2015). The instruments employed are relative gravimeters Scintrex – CG5 and Scintrex CG3+. The gravity data is referenced to the IGSN 71 (International Gravity Standardization Net 71). Positional coordinates are given in the European Terrestrial Reference System 1989 (ETRS89) and refers to the GRS80 ellipsoid. The orthometric heights of the points are obtained during the NVT3 campaign (Kasapovski *et al.*, 2018). The datum of the new levelling network is defined by the fundamental benchmark – Skopje (FRSK) with its orthometric height from NVT2 campaign (AREC, 2019).

Consequently, the gravity data from SFRY were positionally transformed from the old Yugoslav coordinate system to the ETRS89 system, while the transformation from the old Potsdam system to the new IGSN 71 was done by substracting approximately 15 mGal from the gravity data. Since the transformation requires ellipsoidal heights, which were not available at the time, the conversion was performed using geoid undulations from the EGM2008 model to transform the orthometric heights into ellipsoidal heights. For the specific study area, a total of 165 terrestrial gravity data points (104 old points and 61 new points), obtained through relative gravity measurements, are utilized. With a territory covering approximately 900 km², the gravity data density is calculated to be one point per 5.5 km²(R. A. Abbak, 2011). This density is considered sufficient for local geoid determination based on previous research (R. A. Abbak, 2011). In addition to gravity, orthometric and ellipsoidal heights were also collected for these points, which allows for the calculation of geometric geoid undulations. The gravity surveys are processed to calculate gravity anomalies, which form the fundamental input for the geoid computation. The determination of these anomalies requires the application of appropriate gravity reductions and the calculation of normal gravity; these procedures are detailed in the subsequent chapters. The spatial distribution of gravity data points is presented in relation to the topography of the study area in Figure 1.

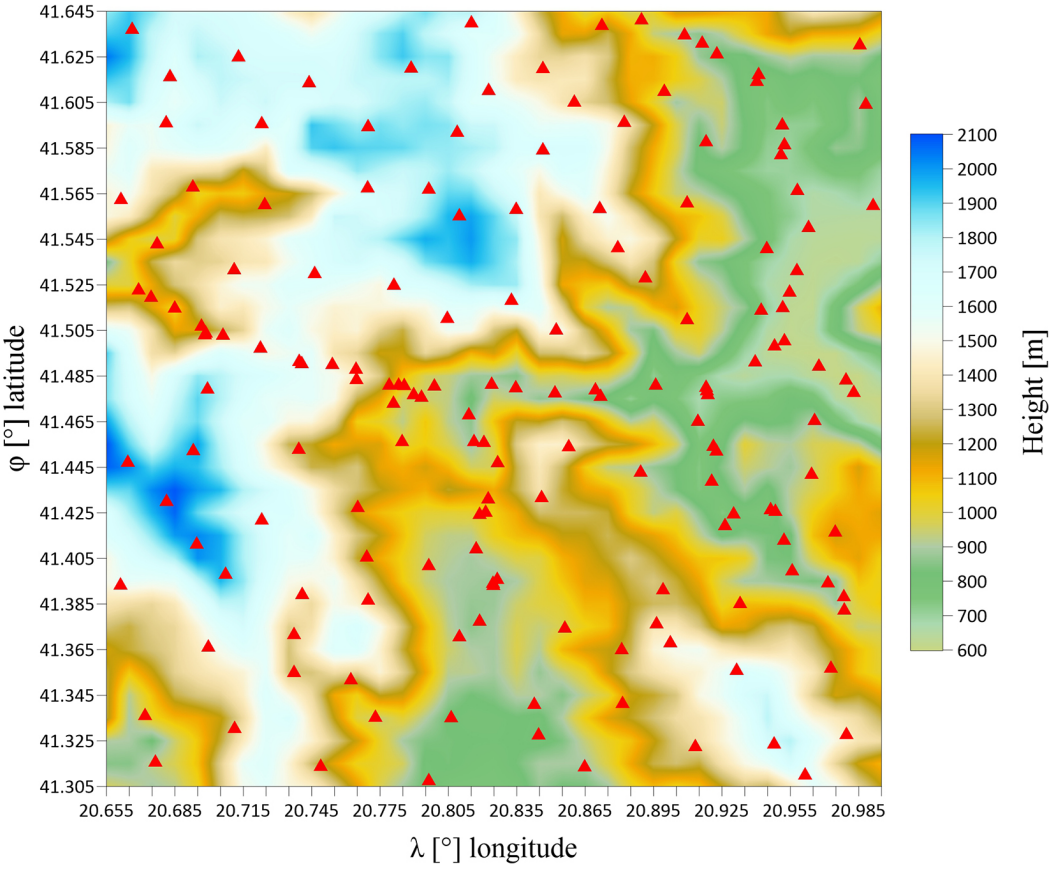

Figure 1: Topography of the study area and spatial distribution of the gravity data

2.1 Global geopotential models

GGMs describe the long-wavelength variations of the Earth's gravity field. They are derived from satellite missions that measure spatial variations in gravity using different satellite configurations. These models are primarily derived from data acquired by dedicated satellite gravity missions—such as CHAMP, GOCE, and GRACE—which measure temporal variations in the gravitational field from space. The construction of GGMs has been an ongoing effort since the 1970s, relying on spherical harmonic expansions of varying degree and order. The earliest models, with maximum degrees around 20, offered limited spatial resolution and were unsuitable for contemporary geodetic and geophysical applications. By contrast, modern GGMs reach degrees and orders up to 5500, allowing for a more refined description of the gravity field. Spherical harmonic terms are classified as zonal, tesseral, or sectoral, depending on their degree and order (Wieczorek & Meschede, 2018). GGMs are generally classified as either satellite-only or combined models that integrate additional altimetry and terrestrial gravity data. This study utilizes satellite-only models from the GOCE and GRACE missions, as well as the combined model EGM2008. The selection criteria prioritised the most recent releases to leverage advancements in processing techniques and data coverage. Table 1 presents the models used in this study:

Table 1: GGMs used in the calculation process

Model name	Year published	N_{max}	Source
Tongji-Grace02k	2018	180	(Q. Chen *et al.*, 2018)
HUST-Grace2016s	2016	160	(Zhou *et al.*, 2017)
GOSG02S	2023	300	(Xinyu; Xu *et al.*, 2023)
GO_CONS_GCF_2_TIM_R6	2019	300	(Brockmann *et al.*, 2021)
GOSG01S	2018	220	(Xinyu Xu *et al.*, 2017)
WHU-SWPU-GOGR2022S	2023	300	(Zhao *et al.*, 2023)
Tongji-GMMG2021S	2022	300	(J. Chen *et al.*, 2022)
ITU_GGC16	2016	280	(Akyilmaz *et al.*, 2016)
EGM2008	2008	2190	(Pavlis *et al.*, 2012)

Before implementation, each GGM requires rigorous validation. This validation generally entails comparing model-derived data such as geometric geoid undulations, free-air anomalies, or Bouguer anomalies. ICGEM service is used for deriving gravimetric geoid undulations from each GGM at its maximum spherical harmonic degree. Validation step for GGMs is needed for obtaining information about the accuracy which they represent geopotential of the Earth. Validation results is important in geoid determination for finding the most optimal GGM for the study area.

The validation was carried out using a network of 46 GNSS/levelling stations which are shown on Figure 2.

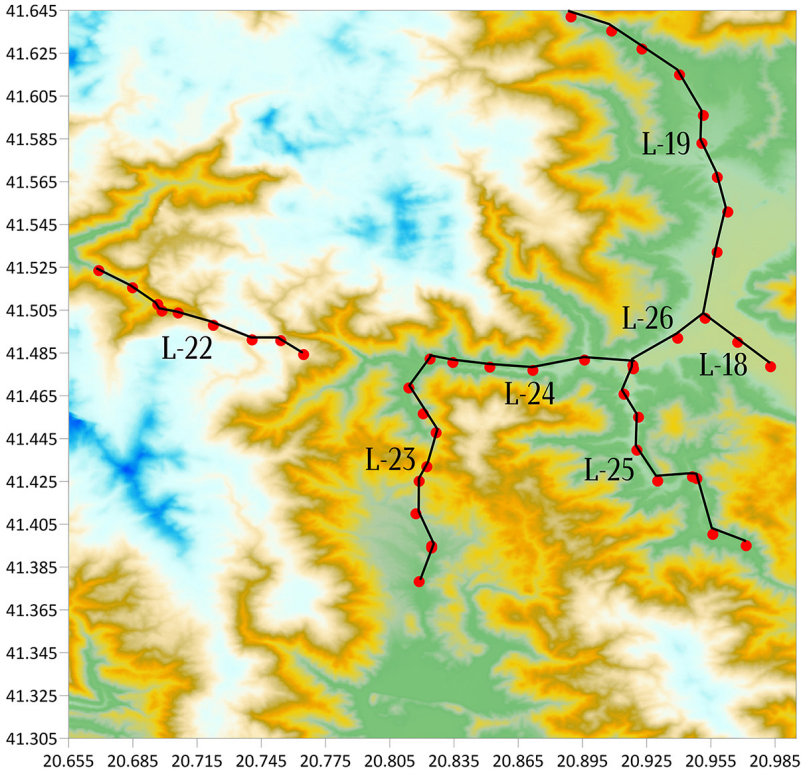

Figure 2: Distribution of the GNSS/levelling points

The results are summarized in Table 2 below:

Table 2: Validation of GGM with GNSS data

Absolute validation of GGM – geoid undulations [cm]						
	no-fit			four-parameter fit		
Name of model	Min.	Max.	RMS	Min.	Max.	RMS
Tongji-Grace02k	-105.48	2.92	30.06	-17.15	20.39	6.44
HUST-Grace2016s	-174.38	-82.78	25.22	-17.10	20.69	6.49
GOSG02S	-39.88	39.61	21.20	-17.20	20.37	6.45
GO_CONS_GCF_2_TIM_R6	-41.38	41.02	22.08	-17.20	20.26	6.41
GOSG01S	-62.48	15.88	21.60	-17.20	20.29	6.39
WHU-SWPU-GOGR2022S	-40.68	38.71	21.21	-17.18	20.40	6.44
Tongji-GMMG2021S	-48.18	32.01	21.30	-17.21	20.70	6.51
ITU_GGC16	-59.48	23.82	22.21	-17.18	20.26	6.41
EGM2008	-55.48	-15.39	8.99	-28.62	15.12	8.27

The comparison indicates that the differences in the no-fit scenario are approximately 21–22 cm, with the combined EGM2008 model resulting in smallest RMS value of 8.99 cm. The Tongji-Grace02k model yielded the highest RMSE. Direct comparisons of geoid undulations reveal systematic biases, resulting in notable RMSE values. To minimise the effect of those types of errors, we must implement a corrector surface, a four-parameter fit (Kotsakis & Sideris, 1999), (Varga, 2018) using Eq. (1):

$$A_i^T \mathrm{x} = x_1 cos\varphi_i cos\lambda_i + x_2 cos\varphi_i sin\lambda_i + x_3 sin\varphi_i cos\lambda_i + x_4 \quad (1)$$

Upon applying a corrector surface, the RMS error is considerably lowered to a consistent value of approximately 6.5 cm across all models. The GOSG01S model performs marginally better than the others, with an RMS of 6.39 cm. It is interesting to note that the EGM2008 which yielded smallest RMS in the no-fit solution, does not have the smallest RMS in the four-parameter fit. Alternative correction surfaces, such as the five-parameter fit (Duquenne *et al.*, 1995) and the seven-parameter fit (Fotopoulos, 2003) were also tested. However, these approaches resulted in higher RMS values. Therefore, the four-parameter fit was adopted for this study.

2.2 Gravity anomalies

Gravity anomalies constitute the second essential dataset for geoid modelling. They are defined as the difference between corrected measurements of gravity at the Earth's surface and the normal gravity on a reference ellipsoid (Heiskanen & Moritz, 1967). While multiple types of gravity anomalies are recognised in physical geodesy, this study focuses on free-air and Bouguer anomalies, which form the basis of the subsequent geoid computations. Before their utilisation, it is critical to describe the gravity reductions applied to the observed data:

– The expression for computing the free-air reduction is calculated with Eq. (2) (Hofmann-Wellenhof & Moritz, 2006):

$$\delta_{gfa} = 0.3086 * \mathrm{H} \quad (2)$$

where H denotes the orthometric height of the point, expressed in meters, while the free-air reduction is in miligals. The reduction values are always positive, except for points located below sea level, where they assume negative values.

– Bouguer reductions are classified as simple or complete, with the simple Bouguer reduction equal in magnitude, but opposite in sign, to the gravitational attraction of the corresponding slab. The formula for computing the simple Bouguer reduction is expressed by Eq. (3):

$$\delta_{gsb} = -2\pi G\rho H \tag{3}$$

The complete Bouguer reduction provides a more accurate representation by initially correcting for the effect of topographic masses and it can calculated using Eq. (4) (Hofmann-Wellenhof & Moritz, 2006):

$$\delta_{gcb} = \delta_{gfa} + \delta_{gsb} + \delta_{gb} = 0.3086 * H - 2\pi G\rho H + \delta_{gt} \tag{4}$$

Eq. (4) is an empirical one, and it is obtained when in Eq. (3) we set the Earth's crust density to $\rho = 2.67\ g/cm^3$.

– Terrain reduction removes the effect of topographic masses near the computation point, considering that the layer between the Earth's surface and the geoid is not a perfect Bouguer slab. Its value is always positive. Here, they are calculated using the *TC* module from Gravsoft software. This is a module that uses rectangular prisms that divide the area around the computational point. In this paper, three *SRTM* models with different resolution were used: detailed (36"), coarse (72") and reference (108"). The radius choice is arbitrary, so the inner zone has radius of $r_1 = 20$ km and the outer zone is defined with $r_2 = 200$ km. The terrain corrections have values from 1.5 to 16.9 mGal, with mean of 6.3 mGal and standard deviation of 2.9 mGal. It must be noted that in both methods, a terrain correction is applied. Here, terrain correction referes as separate input dataset that must be prepared for CSH method.

Having defined the reduction equations, the corresponding expressions for gravity anomalies can now be formulated. With Eq. (5), the free-air anomalies are calculated:

$$\Delta_{fa} = g + \delta_{fa} - \gamma \tag{5}$$

where Δ_{fa} is the free-air anomaly, g is the gravity, δ_{fa} is the free-air reduction, and γ is the normal gravity. The following Eq. (6) is used for the calculation of the Bouguer gravity anomalies:

$$\Delta_b = g + \delta_{fa} + \delta_{gsb} + \delta_{gt} - \gamma \tag{6}$$

where is the gravity, δ_{fa} is the free-air reduction, δ_{gsb} is the simple Bouguer reduction, δ_{gt} is the terrain reduction, and γ is the normal gravity. For defining the normal gravity, we use the Somigliana formula (Somigliana, 1929), (Moritz, 2000) calculated with Eq. (7):

$$\gamma = \frac{a\gamma_o \cos\varphi^2 + b\gamma_p \sin\varphi^2}{\sqrt{a^2 \cos\varphi^2 + b^2 \sin\varphi^2}} \tag{7}$$

where a is the semi-major axis of the ellipsoid, b is the semi-minor axis of the ellipsoid, γ_o is the normal gravity at the equator, γ_p is the normal gravity at the poles, and φ is the geodetic latitude of the point. For this study, we used the GRS80 ellipsoid, consistent with ETRS89 for our region.

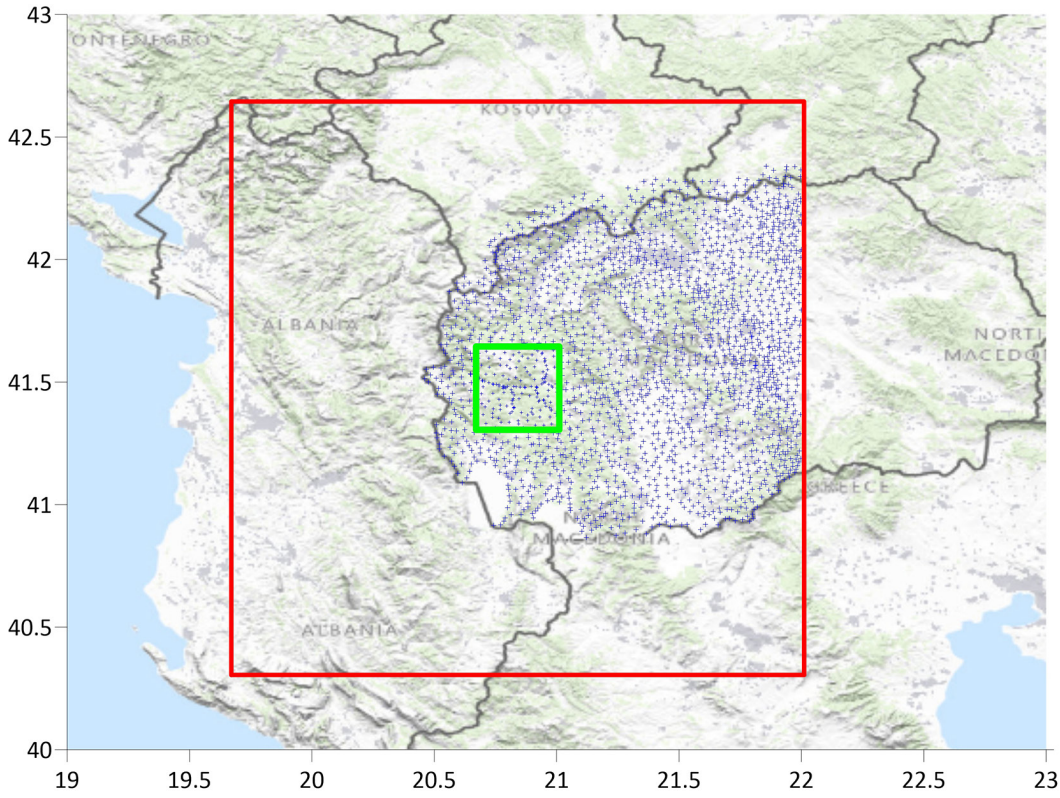

Figure 3: Distribution of free-air anomalies

Initially, the observed gravity values at the 165 gravity stations were converted to free-air anomalies using the corresponding orthometric heights. Subsequently, simple Bouguer anomalies were computed. These anomalies were then interpolated to the grid nodes using an appropriate interpolation method. Based on the Bouguer anomaly values, the mean topography derived from the SRTM dataset was utilized to compute the interpolated free-air anomalies. Accurate geoid determination via the KTH and CSH methods requires free-air anomalies beyond the target area, extending by at least 1° in latitude and longitude. Such data can be collected from neighbouring countries or obtained from GGMs. In our research, we implemented gravity anomalies from the EGM2008 model. Figure 3 shows the free-air anomalies from terrestrial measurements (blue), with the target area marked in green (20'24" latitude and longitude) and the extended data area in red. Terrestrial coverage is adequate in the east, north, and south, whereas the western region (Republic of Albania) is covered solely by EGM2008. The reason why EGM2008 is used is because this model contains the terrestrial gravity data from the region.

In addition to the results in Table 2, where GGM-derived geoid heights were compared with GNSS measurements, a further evaluation was performed using gravity anomalies from GGMs alongside terrestrial free-air and Bouguer anomalies. This comparison gives information about the correlation of the selected GGMs to the ground data, similarly as the comparison of GGMs to the GNSS/levelling data. This comparison employed 165 gravity points, and the results are summarized in Table 3:

Table 3: Validation using free-air and Bouguer anomalies

Absolute validation [mgal] – free-air anomalies				Absolute validation [mgal] – Bouguer anomalies		
Name of model	Min.	Max.	RMS	Min.	Max.	RMS
Tongji-Grace02k	-73.57	108.12	45.65	-31.95	-4.88	20.49
HUST-Grace2016s	-51.48	126.59	51.09	-28.62	-9.46	18.68
GOSG02S	-89.04	85.8	46.03	-23.94	-5.05	13.26
GO_CONS_GCF_2_TIM_R6	-90.25	86.03	46.40	-24.82	-5.19	13.87
GOSG01S	-76.98	91.58	44.65	-25.55	-2.63	13.82
WHU-SWPU-GOGR2022S	-89.06	85.79	46.03	-23.95	-5.07	13.28
Tongji-GMMG2021S	-86.46	87.09	45.54	-23.13	-2.01	11.13
ITU_GGC16	-81.66	93.64	44.64	-30.09	-10.64	18.68
EGM2008	-72.36	84.30	28.61	-66.85	32.95	23.42

As indicated in Table 3, RMS values are greater for free-air anomaly comparisons than for Bouguer anomalies, reflecting the height dependency of both anomaly types. Free-air anomalies are emphasised because they are directly used in geoid determination methods. From the table, it is evident that HUST-Grace2016s performs worst in terms of free-air anomalies, while EGM2008 performs best. Conversely, for Bouguer anomalies, Tongji-GMMG2021S is the most accurate model, whereas EGM2008 shows the largest discrepancies.

2.3 Digital elevation models

DEMs describe the Earth's topography in digital form. DTMs (digital terrain models) reflect the terrain along with vegetation and built structures, while DSMs (digital surface models) represent solely the bare ground, omitting any natural or artificial objects (Varga, 2018). These models are generated through geospatial applications, including gravity interpolation in geodesy, risk assessment in geographic information systems, hydrological simulations, and morphological analyses. Similar to GGMs, DEMs are subject to both random and systematic errors. Therefore, they must be validated against terrestrial data obtained from local surveys before use(Bildirici & Abbak, 2017). In this paper, four different DEMs are used:

– SRTM (Shuttle Radar Topography Mission) is a terrain model created by a joint project between NASA, the German Space Agency, and the Italian Space Agency. With this mission are acquired 3D images of the Earth's surface are acquired using radar interferometry, where with overlapping of two images produces the elevation of the terrain. After that, the images are transformed into a DEM spanning from 60°N to 56°S (Bildirici & Abbak, 2017). The vertical accuracy of the model is approximately 16 meters at around 90% confidence. The products are publicly available at the website of the USGS (USGS, 2024). This model is characterised by a horizontal datum WGS84 and a vertical datum EGM96. The resolution of the used SRTM is 1".
– ASTER (Advanced Space-borne Thermal Emission and Reflection Radiometer) is an observing sensor that was mounted on the satellite Terra in 1999. This sensor is the result of a collaboration between NASA and the Japanese Ministry of Economy, Trade, and Industry (METI). The model is generated by two (a pair) stereo images with nadir and backwards angles over the same area in

2009. This strategy made it possible to obtain DEM with improved accuracy due to multiple images. The model covers the Earth's surface from 83°N to 83°S (Bildirici & Abbak, 2017). Data for the model is available in TIFF format with 1°x1° tiles at 1 arc-second resolution. Model data can be downloaded from the Japanese Space System server (ASTER, 2024). The vertical accuracy ranges from 10 to 20 m. The model has an identical vertical datum, EGM96, and horizontal datum WGS84 as the SRTM models.

– MERIT (Multi-Error-Removed Improved Terrain) is a product of the research team led by Tohishiro Jamazaki from the University of Tokyo. This model has with 3 arc-second resolution (≈90 m), created by using the existing SRTM and AW3D models. These models are improved by removing certain errors (absolute bias, stripe noise, speckle noise, tree height bias) by using multiple satellite databases and filtering techniques. After error removal, the land surfaces had an improved accuracy of around 2 m at a certainty of 58%. The vertical accuracy ranges from 2 m to 5 m. The vertical and horizontal datums remain the same as the two models before. The data is presented in tiles with dimensions of 5°x5°. The format can be ESRI (Fortran Direct Access Format) or GeoTiff. This model finds its application most within projects about hydrology and the environment (Yamazaki *et al.*, 2017).
– TANDEM-X (TerraSAR-X add-on for Digital Elevation Measurements) is an observation radar mission consisting SAR-interferometer created by two identical satellites orbiting closely to each other. The cross-interferometry with distances from 120 to 500 meters makes it possible to create accurate interferograms not affected by time decorrelations or atmospheric influences. The primary aim of the mission is to create a DEM with vertical accuracy of 1-2 meters, which was successfully done. This model finds its use in geology, oceanography, environmental tasks, cartography, and meteorology. The resolution is 1 arc-second (≈30 m). The horizontal datum is WGS84, while the vertical datum is EGM2008 or WGS84. For our paper, EGM2008 was used. As we can see, the vertical datum is different from the previous three models (TanDEM, 2024).

Although these four models have been validated in numerous previous studies, as discussed in the introduction, they have not yet been tested within the territory of the Republic of Macedonia. Therefore, all four models were applied in this research to evaluate their performance. DEMs are widely used in geoid determination, but their performance must be verified against terrestrial measurements. Orthometric heights from the DEMs were compared to 46 GNSS/levelling points. The distribution of the points is shown in Figure 2. The orthometric heights of the levelling points were used. They are obtained with spirit levelling. The accuracy of the GNSS points is 4 mm horizontally and 6 mm vertically as provided by AREC. The comparisons are made between all models and TANDEM-X, because they have different vertical datum, so a correction surface was applied, following the procedure used for GGM evaluations in the previous chapter. The RMS error statistics for all models are summarized in Table 4:

Table 4: Comparison between DEMs

DEM	Absolute validation [m] – four-parameter fit		
	Min.	Max.	RMSE
SRTM-TANDEM	-51.36	41.19	22.25
ASTER-TANDEM	-49.72	43.3	22.68
MERIT-TANDEM	-6.75	31.01	6.85

As noted above, the performance of each model is most effectively assessed by comparing its orthometric heights with GNSS points obtained through spirit levelling. Here, a corrector surface must be implemented since the vertical datum of the DEMs is different from the orthometric heights of the levelling points which are fitted to the mean sea level at a tide gauge. The comparison with terrestrial data provides a quantitative measure of model accuracy, and the results are presented in Table 5:

Table 5: Comparison of DEMs and GNSS points

DEM	Absolute validation [m] – four-parameter fit		
	Min.	Max.	RMSE
SRTM-GNSS	-131.02	134.7	61.21
ASTER-GNSS	-131.53	134.31	61.22
TANDEM-GNSS	-143.19	133.34	59.65
MERIT-GNSS	-142.08	139.04	58.61

Table 5 indicates that RMSE values between the DEMs and terrestrial data range from 58.61 m (MERIT–GNSS) to 61.22 m (ASTER–GNSS). Although MERIT yields the smallest RMS, all four models produce similar results; therefore, all are employed in geoid determination. This indicates that, regardless of the chosen DEM, the resulting geoid model should exhibit minimal RMS error when compared with geometric geoid undulations.

3 Geoid determination methods

The gravimetric geoid can be determined using two methods: KTH and CSH, both relying on similar datasets, including GGMs, DEMs, free-air anomalies, and terrain corrections. The KTH method uses terrestrial free-air anomalies, DEM-based terrain data, and GGM anomalies, while the CSH method additionally incorporates terrain corrections. The methods differ in data processing and Stokes kernel modification: KTH is stochastic, whereas CSH is deterministic. Although both approaches are widely studied, no consensus exists regarding their relative performance, which varies regionally due to differences in terrestrial gravity data, the regional GGM, and the accuracy of GNSS/levelling measurements used for validation.

3.1 KTH method

The KTH method, or least squares modification of the Stokes integral with additive corrections, is a geoid modelling technique developed at the Royal Institute of Technology (KTH), Stockholm, Sweden, by Prof. Lars Sjöberg in the late 1980s. This approach first computes approximate geoid undulations using terrestrial free-air anomalies and GGMs. Additive corrections are then calculated, and their combination with the approximate undulations produces the final gravimetric geoid. The main geoid undulation expression is given in Eq. (8) (L. E. Sjöberg, 2003a):

$$N = \tilde{\mathrm{N}} + \delta N_{top}^{comb} + \delta N_{DWC} + \delta N_{atm} + \delta N_{ell} \tag{8}$$

where $\tilde{\mathrm{N}}$ is the approximate geoid undulation, δN_{top}^{comb} is the combined topography correction, δN_{DWC} is the downward continuation correction, δN_{atm} is the combined atmospheric correction, and δN_{ell} is the ellipsoidal correction. The geoid undulations are calculated using the well-known Stokes formula

Eq. (9), which is one of the fundamental formulas in physical geodesy (Heiskanen & Moritz, 1967):

$$N = \frac{R}{4\pi\gamma}\iint_{\sigma} S(\psi)\Delta g d\sigma \tag{9}$$

Here, Prof. Sjoberg modifies the Stokes kernel (L. E. Sjöberg, 2003a), so basically we calculate the approximate geoid undulations by using the terrestrial free-air anomalies and filling the voids with data from GGM. Now, Eq. (9) can be written as Eq. (10) (L. E. Sjöberg, 2003a):

$$\tilde{N} = \frac{R}{4\pi\gamma}\iint_{\sigma 0} S_L(\psi)\Delta g d\sigma + \frac{R}{2\gamma}\sum_{n=2}^{M} b_n \Delta g_n \tag{10}$$

where Δg is the free-air anomalies, σ_0 is a cap with spherical radius ψ of integration around the computation point, S_L is the modified Stokes kernel, and Δg_n is the gravity anomalies from GGM, b_n is the modification parameter, M is the maximum degree of expansion of the GGM. This modification is necessary because the original Stokes formula assumes gravity measurements over the entire Earth's surface, which is not achievable in practice. Consequently, terrestrial data are used wherever available, while areas without measurements are supplemented using data from GGMs. The Eq. (11) defines the topographic correction that is dependent on the orthometric height of the point, Newtonian gravitational constant and the density of Earth's crust (L. Sjöberg, 2007):

$$\delta N_{comb}^{Top} = \delta N_{dir} + \delta N_{ind}^{Top} = -\frac{2\pi G\rho H^2}{\gamma}\left(1 + \frac{2H}{3R}\right) \tag{11}$$

This correction has the biggest impact of all corrections, with values ranging from centimetres to decimeters. The following correction is the downward continuation correction (L. E. Sjöberg, 2003b):

$$\delta N_{DWC} = \delta N_{dwc}^{(1)} + \delta N_{dwc}^{L1,Far} + \delta N_{dwc}^{L2} \tag{12}$$

where

$$\delta N_{dwc}^{(1)} = \frac{\Delta g_P}{\gamma} H_P + 3\frac{\tilde{N}}{r_p} H_P - \frac{1}{2\gamma}\frac{\partial \Delta g}{\partial r}\Big|_P H_P^2 \tag{13}$$

$$\delta N_{dwc}^{L1,Far} = \frac{R}{2\gamma}\sum_{n=2}^{M} b_n \left[\left(\frac{R}{r_P}\right)^{n+2} - 1\right]\Delta g_n \tag{14}$$

$$\delta N_{dwc}^{L2} = \frac{R}{4\pi\gamma}\iint_{\sigma_0} S^L(\psi)\left[\frac{\partial \Delta g}{\partial r}\Big|_Q \left(H_P - H_Q\right)\right] d\sigma_0 \tag{15}$$

In this correction, the values are in centimetres, which means the influence is smaller than the topographic correction. The combined atmospheric correction (L. E. Sjöberg, 1999) for the masses surrounding the computation point is approximated with Eq. (16):

$$\delta N_{comb}^{Atm} = \frac{GR\rho^a}{\gamma}\iint_{\sigma_0} S^L(\psi) H_P d\sigma_0 \tag{16}$$

Where G is the Newtonian gravitational constant, R is the mean Earth's radius, ρ^a is the density of the atmosphere at sea level, which has a value of 1.23 kg/m^3, S^L is the modified Stokes kernel, H_p is the mean height of the point P, $d\sigma_0$ is surface element on the unit sphere over the integration area σ_0. The

last implemented correction is the ellipsoidal correction (Ellmann & Sjöberg, 2004) because of the approximation of the Earth's surface with a sphere calculated with Eq. (17):

$$\delta N_{ell} \approx \left[\left(0.0036 - 0.0109 \sin^2 \varphi\right)\Delta g + 0.0050 \tilde{N} \cos^2 \varphi\right] Q_0^L \tag{17}$$

The atmospheric and ellipsoidal corrections have magnitudes on the order of millimetres or tenths of a millimetre. Approximate geoid undulations depend on both terrestrial gravity anomalies and GGM-derived anomalies. The topographic correction is determined by the DEM, GGM, and the density of the Earth's crust. Similarly, the downward continuation and atmospheric corrections depend on the DEM, GGM, and terrestrial gravity anomalies. The ellipsoidal correction is computed using the approximate geoid undulations and terrestrial free-air anomalies.

3.2 CSH method

The classical Stokes-Helmert (CSH) method is a deterministic approach for geoid determination. It utilizes the Stokes integral (Eq. 9), solving the global boundary value problem in potential theory (Hofmann-Wellenhof & Moritz, 2005). The method follows a remove–compute–restore (RCR) scheme. In the remove step, DEM and GGM contributions are subtracted from terrestrial free-air anomalies. Helmert's condensation is applied, representing topography as a thin mass layer on the geoid (R. A. Abbak *et al.*, 2024). The DEM and GGM represent the medium and long wavelength variations of the gravity field of the Earth. Residual geoid undulations are computed in the compute step and restored by adding the geoid undulations from DEM and GGM. Residual free-air anomalies are obtained using Eq. (18):

$$\Delta g_{red} = \Delta g^{FA} - \Delta g^{GGM} - \Delta g^{DTE} \tag{18}$$

where Δg^{FA} are the free-air anomalies acquired by terrestrial measurements, Δg^{GGM} are gravity anomalies produced by the GGM, and Δg^{DTE} represent the direct influence of the topographic masses. The Δg^{FA} values are computed using Eq. (5), and the Δg^{GGM} values are obtained using Eq. (19):

$$\Delta g^{GGM} = \frac{GM}{r^2} \sum_{n=2}^{n_{\max}} (n-1) \left(\frac{a}{r}\right)^n \sum_{m=0}^{n} x\left(\Delta \overline{C}_{nm} \cos m\lambda + \overline{S}_{nm} \sin m\lambda\right) \overline{P}_{nm} (\cos\theta) \tag{19}$$

In Eq. (19), GM is the product of the multiplication of the Newtonian gravitational constant and the Earth's mass, r is the radial distance from the computational point, $n_{\max}$ is the maximum degree of expansion, n is the degree of the GGM, m is the order of the GGM, a is the semi-major axis of the level-ellipsoid, $\overline{C}_{nm}$ and $\overline{S}_{nm}$ are harmonic coefficients of the model, and $\overline{P}_{nm}$ is a normalized Legendre function. In the remove step, using the Helmert condensation, the topographic masses are condensed to an infinitely small layer of the geoid and gravity anomalies are continued to the geoid surface from the computation point on the Earth's surface. With this method, certain changes happen in the measurement results, so we have to calculate Δg^{DTE} using Eq. (20) (Serpas, 2004):

$$\Delta g^{DTE} = -\frac{G\rho R^2}{2} \iint_{\sigma} \frac{\left(H_Q - H_P\right)^2}{l_0^3} d\sigma \tag{20}$$

Besides the removal of the direct topographic effect, because of Helmert's condensation, a difference arises between the real and condensed topographic masses, so an additional secondary topographic indirect correction must be applied Δg^{SITE} using Eq. (21) (R. A. Abbak *et al.*, 2024):

$$\Delta g^{SITE} = -\frac{2\pi G\rho H^2}{R} \tag{21}$$

After the corrections for the topographic masses, we must implement a correction for the direct atmospheric effect caused by the atmospheric masses surrounding the point where we do the measurements, so similarly like with the KTH method, we calculate the atmospheric correction Δg^{DAE} using the Eq. (22) (NOAA *et al.*, 1976), (Ramazan Alpay Abbak *et al.*, 2025):

$$\Delta g^{DAE} = 0.871 - 1.0298 \cdot 10^{-4} H + 5.3105 \cdot 10^{-9} H^2 + 2.1642 \cdot 10^{-13} H^3 + 9.5246 \cdot 10^{-18} H^4 \tag{22}$$

The last correction is the ellipsoidal correction, which we add because we do an Earth's approximation with a sphere defined by Eq. (23) (Jekeli, 1981):

$$\Delta g^{ELL} = -\frac{e^2}{R}\sin\theta\cos\theta\frac{\partial T}{\partial\theta} + \frac{e^2}{R}\left(3\cos^2\theta - 2\right)T \tag{23}$$

where e is the first eccentricity of the level ellipsoid, T is the disturbing potential of the computation point, and θ is the co-latitude of the point. With all the aforementioned equations, the final formula for the calculation of the residual of the free-air anomalies is presented in Eq. (24):

$$\Delta g_{red} = \Delta g^{FA} - \Delta g^{GGM} - \Delta g^{DTE} + \Delta g^{SITE} + \Delta g^{DAE} + \Delta g^{ELL} \tag{24}$$

The values of Eq. (24) are used for the calculation of the residuals of the geoid undulations using Eq. (25):

$$N_{\Delta g_{red}} = \frac{R}{4\pi\gamma}\iint_{\sigma} S(\psi)\Delta g_{red}\, d\sigma \tag{25}$$

For obtaining the definitive geoid undulations, we must calculate the geoid undulations from the GGM in the step restore using Eq. (26):

$$Ng^{GGM} = \frac{GM}{\gamma r}\sum_{n=2}^{n_{\max}}\left(\frac{a}{r}\right)^n \sum_{m=0}^{n} x\left(\Delta\bar{C}_{nm}\cos m\lambda + \bar{S}_{nm}\sin m\lambda\right)\bar{P}_{nm}\left(\cos\theta\right) \tag{26}$$

As well as the geoid undulations caused by the topographic masses, which constitute the primary indirect topographic effect on the geoid model using Eq. (27) (L. Sjöberg & Nahavandchi, 1999):

$$N_{PITE} = -\frac{\pi G\rho H^2}{\gamma} - \frac{G\rho R^2}{6\gamma}\iint_{\sigma}\frac{H_Q^3 - H_P^3}{l_0^3} \tag{27}$$

With these three elements, the final formula for the geoid undulations using the CSH method is Eq. (28):

$$\hat{N} = N_{GGM} + N_{\Delta g_{red}} + N_{PITE} \tag{28}$$

4 Practical determination of the geoid models

The geoid computations were performed using the software packages LSMSSOFT (R. Abbak & Üstün, 2015) and CSHSOFT (R. A. Abbak *et al.*, 2024). All input data must share the same grid resolution. For the study area in this paper, a grid resolution of 36 arc seconds (0.01 arc degrees) is selected, corresponding to an approximate 1 km between the grid centres.

– **KTH method** – In this approach, the input data include terrestrial free-air gravity anomalies and gravity anomalies derived from GGM, orthometric heights for the grid centres from DEM, and the

GGM's gfc file containing harmonic coefficients up to the model's maximum degree. Using this method, two geoid models were produced. The first one was obtained using: GGM-GOSG02S, with maximum degree of expansion of 300, DEM-SRTM1", spherical distance of 1 degree and terrestrial gravity anomalies variance of 30 mgal^2. The second one is obtained using model EGM2008 with maximum degree of expansion of 600, while all the other parameters and data used are same as for the first model. Using the specified models and parameters, the smallest RMSE values were obtained, as summarized in Table 6. The resulting geoid model is shown in Figure 4:

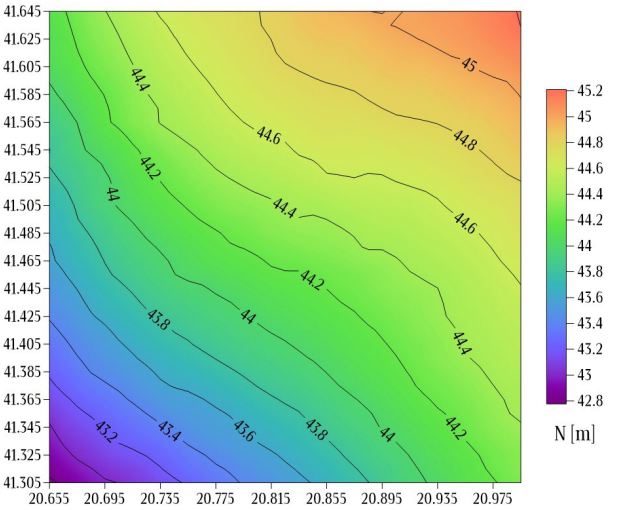

Figure 4: Gravimetric geoid - KTH method (GGM-GOSG02S)

The gravimetric geoid model alone is not directly applicable in practice. It must be aligned with a vertical reference system tied to mean sea level. This requires comparison with a GNSS/levelling geoid model and application of a four-parameter corrector surface that was explained earlier in the paper. The resulting corrections are then added to the gravimetric geoid, producing the final hybrid geoid model. The comparison between the models is presented in Table 6. The first comparison is done directly without applying any corrector surface (no-fit comparison), while the second one is with a four-parameter fit surface. The results show the minimum and maximum difference between the models as well as the RMS error.

Table 6: KTH method comparison

Model	Fit	Absolute validation [cm]		
		Min.	Max.	RMS
GOSG02S	No-fit	32.13	85.57	13.66
	Four-parameter	-21.43	12.47	5.53
EGM2008	No-fit	-18.06	112.86	32.77
	Four-parameter	-24.56	11.54	6.31

– **CSH method –** In this approach, in addition to the data used in the KTH method, terrain corrections are computed using the TC module with GravSoft software (Tscherning *et al.*, 1992), (Forsberg & Tscherning, 2008). Two geoid models were produced using the CSH method, as well. The first one

is created using satellite-only GOSG01S with maximum degree of expansion of 220, and another one using combined EGM2008 model with maximum degree of expansion of 760. The other parameters for both models are DEM-SRTM1", spherical integration distance of 1°, and maximum degree of expansion for Stokes kernel of 160. These GGM models were used since they yielded the smallest RMSE. The final gravimetric geoid model is shown in Figure 5:

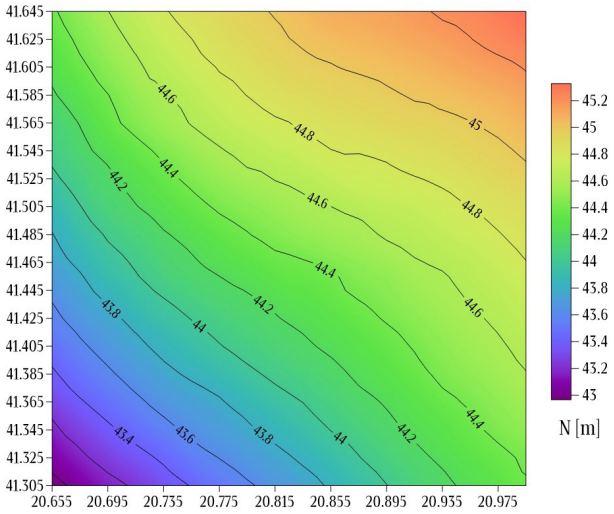

Figure 5: Gravimetric geoid - CSH method (GGM-GOSG01S)

Statistical comparison of the gravimetric and geometric geoid models is done for this method as well, and the results are shown in Table 7:

Table 7: CSH method comparison

Model	Fit	Absolute validation [cm]		
		Min.	Max.	RMS
GOSG01S	No-fit	46.69	100.72	13.70
	Four-parameter	-19.25	14.75	5.51
EGM2008	No-fit	27.46	84.13	14.43
	Four-parameter	-19.45	14.41	5.58

The comparative analysis of the two methods reveals that the optimal performance is achieved using different satellite-only models. Notably, improved results are achieved within the CSH method through the use of an older GGM in comparison with the KTH method. Specifically, GOSG01S, which is the predecessor of GOSG02S, produces slightly smaller RMSE values. Although an older model is employed, this does not imply that the results obtained with GOSG02S are significantly worse. In fact, the differences between GOSG01S and GOSG02S are on the order of tenths of a millimeter. Here, only the model yielding the smallest RMSE is presented.

Another comparison is done by presenting the differences between the models derived with both methods. The check is done on the 46 GNSS/levelling points. The results are presented in Table 8.

Table 8: Statistics of differences between KTH and CSH models

Model	Absolute validation [cm]			
	Min.	Max.	Mean	RMS
Gravimetric	-19.30	-12.06	-15.09	1.21
Hybrid	-5.45	2.65	-0.47	1.55

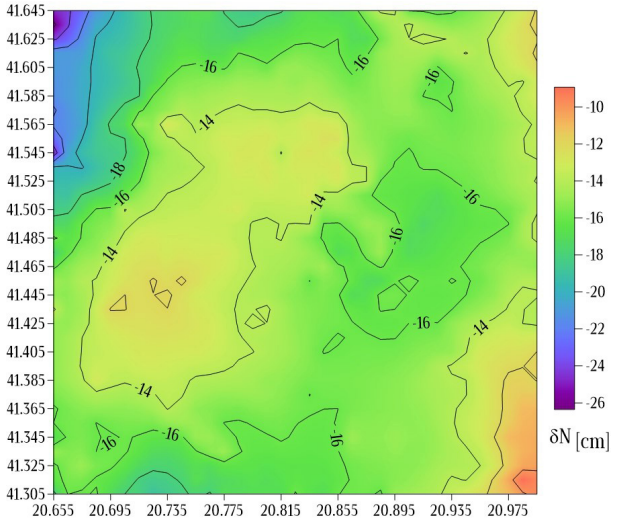

Figure 6: Gridded differences between KTH and CSH methods, gravimetric geoid

As illustrated in Figure 6, the gridded differences are smaller in the southeastern part of the study area. Moving toward the northwestern region, these differences increase between the two methods. This variation is likely attributed to the more pronounced topographic relief present in the northwestern portion of the study area. To assess the true performance of a geoid model using GNSS-levelling data, an additional validation is carried out in a relative sense. In this approach, discrepancies between differential geoid heights derived from gravimetric and geometric geoid models are computed for all possible baselines formed by the GNSS-levelling benchmarks. The resulting disagreements are then expressed in relative terms, specifically in parts per million (ppm), by fitting the gravimetric geoid to the GNSS-levelling geoid with the Eq. (29):

$$\Delta N_{ij} = \frac{\left| N_i^{gra} + a_i^T x - N_j^{gra} + a_j^T x - \left(N_i^{geo} - N_j^{geo} \right) \right|}{D_{ij}} \tag{29}$$

where D_{ij} is the spherical distance expressed in kilometers between points i and j, N_i^{gra} and N_j^{gra} are the gravimetric geoid undulations and N_i^{geo} and N_j^{geo} are the geometric geoid undulations. The geoid undulations are expressed in millimeters.

Table 9: Statistics of relative validation with KTH and CSH models

Model	Relative validation [ppm]		
	Minimum	Maximum	Mean
KTH	0.0	365.2	7.6
CSH	0.0	352.2	7.1

Examination of the final geoid models reveals similar behaviour between the gravimetric and hybrid models for both KTH and CSH methods, as summarized in Table 10.

Table 10: Comparison of models between methods

Model	Units - [m]		
	Minimum	Maximum	Range
KTH-gravimetric	42.78	45.21	2.43
CSH-gravimetric	42.97	45.33	2.36
KTH-hybrid	42.38	44.17	1.79
CSH-hybrid	42.46	44.14	1.68

Both approaches yielded accurate results, with RMS values of 5.53 cm for KTH and 5.51 cm for CSH, indicating that the CSH hybrid model represents the most precise solution.

5 Conclusion

From the preceding discussion, it is evident that validation of GGMs is a crucial step before their use in geoid determination. Similarly, terrestrial gravity anomalies, obtained from field measurements, provide ground-truth data, and the reliability of the resulting geoid model improves with the quantity and quality of such data. DEMs must also be validated against orthometric heights acquired through spirit levelling before application. Also, the use of satellite-only models exhibited smaller RMS error values than using EGM2008 model for the KTH method, while for the CSH method, both types of GGMs showed similar behavior.

Since this represents the first study of its kind conducted within the Republic of Macedonia, several directions for future research are proposed to enhance the accuracy and reliability of geoid modelling in the region:

- Future studies may employ different crustal density models, such as the UNB model, to assess their influence on the computed geoid and improve regional representation of mass distribution.
- The use of combined geoid models should be explored for validation against ground-truth GNSS/levelling data and to refine local geoid computations.
- Utilization of high-resolution DEMs, such as FABDEM or Fathom DEM, could replace or supplement data to improve the modelling of topographic effects, particularly in regions with complex relief.
- Application of another RCR methods such as implementation of least squares collocation (LSC) or Fast Fourier Transform (FFT) methods—may yield higher precision in local geoid determination.
- Future campaigns could focus on densifying the existing gravity network, particularly by conducting additional relative gravity measurements to complement the data obtained during the 2013 campaign. Using a consistent and recent gravity dataset exclusively for geoid computation would enhance the internal consistency and accuracy of the model.

Literature and references

Abbak, R., & Üstün, A. (2015). A software package for computing a regional gravimetric geoid model by the KTH method. Earth Science Informatics, 8, 255-265. DOI:10.1007/s12145-014-0149-3

Abbak, R. A. (2011). Evaluation of Global Earth Potential Models Using Spectral Methods and Local Improvement for Geoid Determination. (PhD). Selcuk University, Konya, Turkey.

Abbak, R. A. (2014). Effect of ASTER DEM on the prediction of mean gravity anomalies: a case study over the Auvergne test region. Acta Geodaetica et Geophysica, 49. DOI:10.1007/s40328-014-0062-8

Abbak, R. A., Erol, B., & Ustun, A. (2012). Comparison of the KTH and remove–compute–restore techniques to geoid modelling in a mountainous area. Computers & Geosciences, 48, 31-40. DOI:10.1016/j.cageo.2012.05.019

Abbak, R. A., Goyal, R., & Ustun, A. (2024). A user-friendly software package for modelling gravimetric geoid by the classical Stokes-Helmert method. Earth Science Informatics, 17(4), 3811-3824. DOI:10.1007/s12145-024-01328-0

Abbak, R. A., Goyal, R., Ustun, A., & Olgun, S. (2025). Combined effects of terrain corrections and deterministic modifiers on the Stokes-Helmert geoid over sophisticated topography. Acta Geodaetica et Geophysica, 60(1), 29-51. DOI:10.1007/s40328-025-00460-7

Akyilmaz, O., Ustun, A., Aydin, C., Arslan, N., Doganalp, S., Guney, C., . . . Yagci, O. (2016). High Resolution Gravity Field Determination and Monitoring of Regional Mass Variations using Low-Earth Orbit Satellites.

AREC. (2019). National Report - Republic of North Macedonia.

ASTER. (2024). ASTER. https://gdemdl.aster.jspacesystems.or.jp/.

Bako, M., Elsaka, B., Kusche, J., & Fenoglio-Marc, L. (2025). Evaluation of GOCE/GRACE and combined global geopotential models using GNSS/levelling data over Nigeria. Studia Geophysica et Geodaetica, 69(1), 1-21. DOI:10.1007/s11200-023-0804-6

Bildirici, İ. Ö., & Abbak, R. A. (2017). Comparison of Aster and Srtm Digital Elevation Models at One-Arc-Second Resolution over Turkey. Selcuk University Journal of Engineering ,Science and Technology, 5(1), 16-25. DOI:10.15317/Scitech.2017.66

Brockmann, J. M., Schubert, T., & Schuh, W.-D. (2021). An Improved Model of the Earth's Static Gravity Field Solely Derived from Reprocessed GOCE Data. Surveys in Geophysics, 42(2), 277-316. DOI:10.1007/s10712-020-09626-0

Chen, J., Zhang, X., Chen, Q., Shen, Y., & Nie, Y. (2022). Static Gravity Field Recovery and Accuracy Analysis Based on Reprocessed GOCE Level 1b Gravity Gradient Observations. Paper presented at the EGU General Assembly 2022, Vienna, Austria.

Chen, Q., Shen, Y., Francis, O., Chen, W., Zhang, X., & Hsu, H. (2018). Tongji-Grace02s and Tongji-Grace02k: High-Precision Static GRACE-Only Global Earth's Gravity Field Models Derived by Refined Data Processing Strategies. Journal of Geophysical Research: Solid Earth, 123(7), 6111-6137. DOI:https://doi.org/10.1029/2018JB015641

Duquenne, H., Jiang, Z., & Lemarié, C. (1995, 1995//). Geoid Determination and Levelling by GPS: Some Experiments on a Test Network. Paper presented at the Gravity and Geoid, Berlin, Heidelberg.

Ellmann, A., & Sjöberg, L. E. (2004). Ellipsoidal correction for the modified Stokes formula. Boll Geod Sci Aff(No. 3).

Forsberg, R., & Tscherning, C. C. (2008). An overview manual for the GRAVSOFT Geodetic Gravity Field Modelling Programs

Fotopoulos, G. (2003). An analysis on the optimal combination of geoid, orthometric and ellipsoidal height data. (PhD).

Godah, W., Krynski, J., & Szelachowska, M. (2015). On the accuracy assessment of the consecutive releases of GOCE-based GGMs over the area of Poland. Newton's Bulletin, 49-62.

Gospodinov, S., Peneva, E., Penev, P., Sechkov, K., Dimeski, S., & Starchevich, M. (2015, 17-21 May 2015). Basic Gravimetric Network of Republic Macedonia - a new reality. Paper presented at the FIG Working Week 2015 - From the Wisdom of the Ages to the Challenges of the Modern World, Sofia, Bulgaria.

Halim, S. M. A., Green, M. F. P., Narashid, R. H., & Din, A. H. M. (2019, 2-3 Aug. 2019). Accuracy Assessment of TanDEM-X 90 m Digital Elevation Model In East of Malaysia Using GNSS/Levelling. Paper presented at the 2019 IEEE 10th Control and System Graduate Research Colloquium (ICSGRC).

Heiskanen, A. W., & Moritz, H. (1967). Physical geodesy: W. H. Freeman and Co Ltd.0716702339.

Hofmann-Wellenhof, B., & Moritz, H. (2005). Physical Geodesy. Austria

Hofmann-Wellenhof, B., & Moritz, H. (2006). Physical Geodesy. Austria: SpringerWienNewYork

ICGEM. (2025). Static Models. https://icgem.gfz-potsdam.de/tom_longtime

Ince, E. S., Barthelmes, F., Reißland, S., Elger, K., Förste, C., Flechtner, F., & Schuh, H. (2019). 15 years of successful collection and distribution of global gravitational models, associated services and future plans. - Earth System Science Data.

Jekeli, C. (1981). The Downward Continuation to the Earth's Surface of Truncated Spherical and Ellipsoidal Harmonic Series of the Gravity and Height Anomalies. (PhD). The Ohio State University, Ohio, Columbus.

Kasapovski, F., Gospodinov, S., Srbinoski, Z., Dimov, L., Bogdanovski, Z., & Gegovski, T. (2018). Vertical Crustal Movements in Seismic Active Regions. Scientific Journal of Civil Engineering, 7(2).

Kotsakis, C., & Sideris, M. G. (1999). On the adjustment of combined GPS/levelling/geoid networks. Journal of Geodesy, 73(8), 412-421. DOI:10.1007/s001900050261

Krdžalić, D., & Abbak, R. A. (2023). A precise geoid model of Bosnia and Herzegovina by the KTH method and its validation. Survey Review, 55(393), 513-523. DOI:10.1080/00396265.2022.2163361

Moritz, H. (2000). Geodetic Reference System 1980. Journal of Geodesy, 74(1), 128-133. DOI:10.1007/s001900050278

NOAA, NASA, & USAF. (1976). US standard atmosphere.US Government Printing Office. Washington DC.

Pavlis, N. K., Holmes, S. A., Kenyon, S. C., & Factor, J. K. (2012). The development and evaluation of the Earth Gravitational Model 2008 (EGM2008). Journal of Geophysical Research: Solid Earth, 117(B4). DOI:https://doi.org/10.1029/2011JB008916

Serpas, J. G. (2004). The Direct Effect on Geoid Computations. Uniciencia 21, 21, 145-149.

Sjöberg, L. (2007). The topographic bias by analytical continuation in physical geodesy. Journal of Geodesy, 81, 345-350. DOI:10.1007/s00190-006-0112-2

Sjöberg, L., & Nahavandchi, H. (1999). On the indirect effect in the Stokes–Helmert method of geoid determination. Journal of Geodesy, 73, 87-93. DOI:10.1007/s001900050222

Sjöberg, L. E. (1999). The IAG approach to the atmospheric geoid correction in Stokes' formula and a new strategy. Journal of Geodesy, 73(7), 362-366. DOI:10.1007/s001900050254

Sjöberg, L. E. (2003a). A general model for modifying Stokes' formula and its least-squares solution. Journal of Geodesy, 77(7), 459-464. DOI:10.1007/s00190-003-0346-1

Sjöberg, L. E. (2003b). A solution to the downward continuation effect on the geoid determined by Stokes' formula. Journal of Geodesy, 77(1), 94-100. DOI:10.1007/s00190-002-0306-1

Somigliana, C. (1929). Teoria generale del campo gravitazionale dell'ellissoide di rotazione. Memorie della Società Astronomia Italiana, 4.

TanDEM. (2024). TanDEM-X Global Digital Elevation Model (DEM). . https://tandemx-science.dlr.de/

Tscherning, C. C., Forsberg, R., & Knudsen, P. (1992). The GRAVSOFT package for geoid determination. Continued Workshop on the European Geoid.

USGS. (2024). https://earthexplorer.usgs.gov/

Varga, M. (2018). The Application of Crustal Models in Regional Modelling of the Earth's Gravity Field.

Wieczorek, M. A., & Meschede, M. (2018). SHTools: Tools for Working with Spherical Harmonics. Geochemistry, Geophysics, Geosystems, 19(8), 2574-2592. DOI:https://doi.org/10.1029/2018GC007529

Xu, X., Li, J., Zhao, Y., & Wei, H. (2023). A GOCE only gravity model GOSG02S based on the SGG and SST observations.

Xu, X., Zhao, Y., Reubelt, T., & Tenzer, R. (2017). A GOCE only gravity model GOSG01S and the validation of GOCE related satellite gravity models. Geodesy and Geodynamics, 8(4), 260-272. DOI:https://doi.org/10.1016/j.geog.2017.03.013

Yamazaki, D., Ikeshima, D., Tawatari, R., Yamaguchi, T., O'Loughlin, F., Neal, J. C., . . . Bates, P. D. (2017). A high-accuracy map of global terrain elevations. Geophysical Research Letters, 44(11), 5844-5853. DOI:https://doi.org/10.1002/2017GL072874

Yilmaz, M., Turgut, B., Gullu, M., & Yilmaz, I. (2016). EVALUATION OF RECENT GLOBAL GEOPOTENTIAL MODELS BY GNSS/LEVELLING DATA: INTERNAL AEGEAN REGION. International Journal of Engineering and Geosciences, 1, 15-19. DOI:10.26833/ijeg.285221

Zhao, Y., Li, J., Xu, X., & Su, Y. (2023). WHU-SWPU-GOGR2022S: A combined gravity model of GOCE and GRACE.

Zhou, H., Luo, Z., Zhou, Z., Zhong, B., & Hsu, H. (2017). HUST-Grace2016s: A new GRACE static gravity field model derived from a modified dynamic approach over a 13-year observation period. Advances in Space Research, 60(3), 597-611. DOI:https://doi.org/10.1016/j.asr.2017.04.026

Petrovski F., Bogdanovski Z. (2026). Comparison of Local Geoid Models in Western Macedonia Determined by KTH and CSH Methods.
Geodetski vestnik, 70 (2), 248-267.
DOI: https://doi.org/geodetski-vestnik.2026.02.248-267

Msc. Filip Petrovski, Teaching Assistant,
Faculty of Civil Engineering,
Ss. Cyril and Methodius – Skopje, N. Macedonia,
e-mail: petrovski@gf.ukim.edu.mk

prof. Zlatko Bogdanovski,
Faculty of Civil Engineering,
Ss. Cyril and Methodius – Skopje, N. Macedonia,
e-mail: bogdanovski@gf.ukim.edu.mk